Earth and Planetary Science Letters
January 2009, Volume 277, Issues 3-4, Pages 318-326
http://dx.doi.org/10.1016/j.epsl.2008.10.028

Hf and Nd isotopes in marine sediments: Constraints on global silicate weathering

G. Bayon[a, *], K.W. Burton[b, c], G. Soulet[a, d], N. Vigier[e], B. Dennielou[a], J. Etoubleau[a], E. Ponzevera[a], C.R. German[f] and R.W. Nesbitt[g]

[a] Département Géosciences Marines, Ifremer, 29280 Plouzané, France
[b] Department of Earth Sciences, The Open University, Walton Hall, MK7 6AA Milton Keynes, UK
[c] Department of Earth Sciences, Oxford University, Parks Road, OX1 3PR Oxford, UK
[d] CEREGE, Université Paul-Cézanne Aix-Marseille 3, Europôle de l'Arbois BP80, 13545 Aix-en-Provence Cedex 4, France
[e] CRPG, 15 rue Notre Dame des Pauvres, 54501 Vandoeuvre-les-Nancy, France
[f] Woods Hole Oceanographic Institution, Woods Hole, MA 02543, USA
[g] National Oceanography Centre, Southampton, Empress Dock, SO14 3ZH, Southampton, UK

*: Corresponding author : G. Bayon, Tel.: +33 2 98 22 46 30; fax: +33 2 98 22 45 70, email address : Germain.Bayon@ifremer.fr

Abstract:

The combined use of Lu–Hf and Sm–Nd isotope systems potentially offers a unique perspective for investigating continental erosion, but little is known about whether, and to what extent, the Hf–Nd isotope composition of sediments is related to silicate weathering intensity. In this study, Hf and Nd elemental and isotope data are reported for marine muds, leached Fe-oxide fractions and zircon-rich turbidite sands collected off the Congo River mouth, and from other parts of the SE Atlantic Ocean. All studied samples from the Congo fan (muds, Fe-hydroxides, sands) exhibit indistinguishable Nd isotopic composition (εNd ~ − 16), indicating that Fe-hydroxides leached from these sediments correspond to continental oxides precipitated within the Congo basin. In marked contrast, Hf isotope compositions for the same samples exhibit significant variations. Leached Fe-hydroxide fractions are characterized by εHf values (from − 1.1 to + 1.3) far more radiogenic than associated sediments (from − 7.1 to − 12.0) and turbidite sands (from − 27.2 to − 31.6). εHf values for Congo fan sediments correlate very well with Al/K (i.e. a well-known index for the intensity of chemical weathering in Central Africa). Taken together, these results indicate that (1) silicate weathering on continents leads to erosion products having very distinctive Hf isotope signatures, and (2) a direct relationship exists between εHf of secondary clay minerals and chemical weathering intensity.

These results combined with data from the literature have global implications for understanding the Hf–Nd isotope variability in marine precipitates and sediments. Leached Fe-hydroxides from Congo fan sediments plot remarkably well on an extension of the 'seawater array' (i.e. the correlation defined by deep-sea Fe–Mn precipitates), providing additional support to the suggestion that the ocean Hf budget is dominated by continental inputs. Fine-grained sediments define a diffuse trend, between that for igneous rocks and the 'seawater array', which we refer to as the 'zircon-free sediment array' (εHf = 0.91 εNd + 3.10). Finally, we show that the Hf–Nd arrays for seawater, unweathered igneous rocks, zircon-free and zircon-bearing sediments (εHf = 1.80 εNd + 2.35) can all be reconciled, using Monte Carlo simulations, with a simple weathering model of the continental crust.

Keywords: neodymium isotopes; hafnium isotopes; silicate weathering; continental erosion; seawater array; Congo fan

1 – Introduction

Chemical weathering of silicate rocks represents an important sink for atmospheric CO_2 on geological timescales, and hence is thought to have played a significant role in regulating Earth's climate (Walker et al., 1981; Berner et al., 1983; Raymo et al., 1988). Despite the potential importance of this process, our ability to reconstruct past variations in silicate weathering remains limited. Many attempts to investigate changes in silicate weathering intensity over time have focused upon measurements of radiogenic isotope ratios in ancient seawater records (Edmond, 1992; Raymo and Ruddiman, 1992; Ravizza and Peucker-Ehrenbrink, 2003; Foster and Vance, 2006). Analysis of sediment records also offers opportunity to assess climatic controls on continental erosion over variable timescales (Jung et al., 2004; Clift et al., 2005, 2008). However, deconvolving the silicate weathering signal from both marine and sediment records is difficult using conventional geochemical proxies, because measured variations can reflect either changes in source, physical erosion, or chemical weathering. A proxy which would allow one to reconstruct past continental erosion signals independently, and to directly compare records acquired from different geographic locations, would offer a new insight into our understanding of how climate change, crustal weathering and ocean chemistry are linked. The use of non-conventional stable isotope tracers (e.g. Li), which are not affected significantly by variations in sediment provenance, bring useful complementary information (Huh et al., 2004; Vigier et al., 2008), but their utility as weathering proxies is yet to be fully understood.

The combined use of Lu-Hf and Sm-Nd isotope systems offers a unique perspective on silicate weathering. On a global scale, these two isotope systems behave similarly during magmatic processes. This is clearly illustrated by the broadly coherent correlation between Nd and Hf isotopes, the so-called 'terrestrial array' (Vervoort et al., 1999), defined by most ocean basalts, continental crustal rocks and sediments. However, significant differences between the two Lu-Hf and Sm-Nd pairs are evident at the mineral scale. While Sm and Nd are incorporated in similar proportions in most common rock-forming minerals, Lu and Hf are partitioned differently into each mineral phase. The relatively large degree of fractionation between Lu and Hf during magmatic crystallization leads, with time and radioactive decay of ^{176}Lu to ^{176}Hf, to minerals having very distinctive Hf isotopic signatures. This decoupling between Lu-Hf and Sm-Nd systems at the mineral scale hence provides a potential means for tracing silicate weathering, i.e. a process which does not affect the whole rock uniformly, but only selected mineral phases.

On the continents, silicate weathering typically produces a dissolved fraction, secondary clay minerals and residual fine and coarse-grained sediments. A large proportion of the Hf inventory in crustal rocks remains locked in zircons during weathering, a mineral with very low Lu/Hf ratios that is highly resistant to physical and chemical weathering, and which tends to be sorted into silt and sand fractions during sediment transport (Patchett et al., 1984). The comprehensive studies of Patchett et al. (1984) and Vervoort et al. (1999) have shown clearly that this 'zircon effect' leads to significant decoupling of Hf-Nd in the sedimentary system. An understanding of the sensitivity of Hf isotopes to silicate weathering has also been gained from the study of deep-sea ferromanganese crusts and nodules. Investigations of marine Fe-Mn deposits have shown that the deep ocean is characterized by radiogenic (high) Hf isotope compositions (ε_{Hf} from ~ -2 to +6), defining a 'seawater array' on a Hf-Nd isotope diagram that is distinct from the 'terrestrial array' (Albarède et al., 1998). Although a number of studies have suggested that contributions from submarine hydrothermal systems could play an important role in the dissolved Hf budget of the ocean (White et al., 1986; Godfrey et al., 1997; Bau and Koschinsky, 2006), other work has indicated that such high $^{176}Hf/^{177}Hf$ ratios in seawater could be acquired instead through dissolution of the zircon-free component of continental rocks during crustal weathering (Piotrowski et al., 2000; van de Flierdt et al., 2002, 2004, 2007). Van de Flierdt et al. (2007) recently proposed, based on mass balance calculations between a low ε_{Hf} zircon reservoir and a high ε_{Hf} non-zircon reservoir, that the 'seawater array' could be explained solely by incongruent weathering of continental rocks. New evidence from leachate experiments of silicate rocks and analysis of river waters provides direct support for this latter hypothesis, by demonstrating that preferential dissolution of minerals with high Lu/Hf ratios (e.g. apatite, sphene) versus more resistant minerals (e.g. feldspar, zircon) releases a radiogenic fraction of dissolved Hf to rivers (Bayon et al., 2006). In their study, Bayon et al. (2006) also provided an estimate for the overall global riverine ε_{Hf} input to the Atlantic Ocean, found to match the ε_{Hf} range for Atlantic deep-waters recorded by marine ferromanganese deposits, consistent with the suggestion that riverine input dominates the oceanic Hf budget.

In principle, changes in the intensity of physical or chemical weathering will result in variations in the Hf isotope composition of both the dissolved load and residual sediments. However, at this stage little is known on whether, and to what extent, Hf-Nd isotope compositions of sediments relate to silicate weathering intensity, because there is a limited

amount of available data for Hf and Nd isotopic compositions in marine sediments. Recent studies have reported deep-sea sediments exhibiting higher Hf ratios than other rocks at a given Nd ratio, but the significance of those high ε_{Hf} values is unclear (Pettke et al., 2002; Chauvel et al., 2008). While zircon-rich sandy fractions are generally sequestered on continents or continental margins, fine particles can be exported efficiently to the deep ocean via riverine or aeolian transport, and ocean circulation. Hence, Hf-Nd isotope systematics in deep-sea sediment records could provide useful information on past weathering conditions on continents.

Here, we report Hf and Nd elemental and isotope data for a series of marine muds, leached Fe-Mn oxide fractions and zircon-bearing turbidite sands collected close to the mouth of the Congo River, in addition to a series of hemipelagic sediments recovered from other parts of the SE Atlantic Ocean. These results provide additional constraints on the behavior of Hf isotopes during continental weathering, which further demonstrate the utility of the Hf-Nd isotope pair proxy. It is shown that the global Hf-Nd isotope variability observed for igneous rocks, sands, marine sediments and Fe-oxide precipitates can be explained by a simple weathering model of the upper continental crust.

2 – Samples and methods

Samples analysed in this study are from three different areas in the SE Atlantic Ocean (Congo deep-sea fan, Angola Basin, Cape Basin; Fig. 1). Sediment cores collected off the Congo River were recovered during the ZaiAngo project (Savoye et al., 2000). KZAI-1 is a 10-meter-long core located on the northern slope of the Congo deep-sea fan, at ~ 800 m water depth, which provides a continuous record of the Congo sediment discharge for the last 40,000 years (F. Jansen, pers. comm.). Granulometric measurements indicate that grain-size is broadly homogeneous throughout the whole core, with medians ranging between 4 and 6 µm. A total of ten sediment samples from KZAI-1, collected at various core depths, were analysed for this study. Hf-Nd isotope analyses were performed on both bulk sediment samples and leached Fe-hydroxide fractions. A few coarse-grained turbidite layers collected from three cores (KZAI-5/8/13) recovered in the canyon system and associated lobes were also analysed (Fig. 1). These samples correspond to silt and fine sand sediments, with medians averaging ~ 40 µm. Cores from the Angola Basin (MD96-2091; 3570m water depth) and Cape Basin (MD96-2085, 3000m; MD96-2086, 3600m; MD96-2098, 2900m; MD96-

2087, 1030m) were retrieved during the IMAGES II-Nausicaa cruise (1996). Their lithologies are variable down-core, exhibiting changes in the relative amount of carbonate ooze, biogenic silica and detrital material (Bayon et al., 2003; Bertrand et al., 2003; Pichevin et al., 2004). With the exception of core MD96-2087 data, all Nd isotope data reported in this study for these SE Atlantic cores are from Bayon et al. (2003).

All sediments were dissolved either in steel-jacketed Teflon bombs, using HF-$HClO_4$ mixtures, or by alkaline fusion (Bayon et al., 2008). Both procedures ensure complete sample digestion, including the dissolution of highly resistant minerals such as zircons. The Fe-Mn oxide component of Congo fan fine sediments (KZAI-1) was leached either using a mixed solution of hydroxylamine hydrochloride and acetic acid (referred to as 'HH solution' from herein), or with diluted HNO_3 solutions (0.2M) at room temperature, after removal of carbonate and organic fractions using acetic acid and hydrogen peroxide solutions, respectively. This latter procedure differs from those reported in previous studies (e.g. Bayon et al., 2002; Gutjahr et al., 2007), which involve the use of HH solutions to extract the radiogenic isotope signals of e.g. Nd, Pb and Th from Fe-Mn oxyhydroxide coatings. During the course of our experimental work, however, leaching with HH solutions was found not to work for Hf isotopes. Hafnium is a very insoluble element that adsorbs efficiently onto particles. Most likely, a significant fraction of the oxide-hosted Hf dissolved using HH was re-adsorbed onto clay particles during the leaching step. Therefore, we modified our leaching procedure and performed a series of tests using of diluted HCl and HNO_3 solutions. Our experimental results show that the Hf isotopic signatures extracted using HH and 0.2M HNO_3 (Table 1), and 0.2M HCl (data not shown here) are all similar within error, but that the precision on measured isotopic ratios is significantly improved for HNO_3 leachates (Table 1). This indicates that re-adsorption of dissolved Hf onto clay particles is probably reduced when leaching with nitric acid. Importantly, however, the agreement between the data obtained on both HH and HNO_3 leachates suggests that leaching with diluted HNO_3 do not lead to any measurable dissolution of detrital particles. This provides reassuring evidence that the Hf isotope signal extracted with diluted nitric solution corresponds to the pristine Hf fraction hosted by sedimentary Fe-Mn oxides.

The bulk major element composition of our SE Atlantic sediments was determined by wavelength-dispersive X-ray fluorescence (WD-XRF) analysis of fusion beads. XRF data are not listed here, but are available from the authors upon request. Hafnium and REE concentrations in sediment samples were analysed using three different ICP-MS (VG

Plasmaquad II+, Agilent 7500s, and Element2). The precision on measured concentrations was typically better than 5% for Sm, Nd and Hf, and better than 10%, in most cases, for Lu. Details on analytical techniques for Hf and Nd separation chemistries and isotope measurements can be found elsewhere (Chu et al., 2002; Bayon et al., 2006). Hafnium isotope analyses were performed using two different MC-ICP-MS instruments at The Open University (Nu Plasma, Nu Instruments) and at IFREMER (Neptune, Thermo Fischer Scientific). Nd isotopic ratios were determined at IFREMER either by TIMS (Finnigan MAT261) or by Neptune MC-ICP-MS. For the sediments, analysis of the JMC475 standard during the analytical sessions gave $^{176}Hf/^{177}Hf$ of 0.282160 ± 0.000022 (2 s.d., n=20) and 0.282151 ± 0.000010 (2 s.d., n=9), on the Nu Plasma and Neptune instruments, respectively. The external reproducibility of Hf isotope analyses for Fe-hydroxide fractions was assessed by analysing small volumes (30-200 μl) of JMC475 Hf standard solution repeatedly (i.e. analysis of ~1 to 4ng Hf), giving 2sd = ± 0.000044 ppm for ^{177}Hf ion beam signals > 0.8V. Analysis of the JNdi-1 standard during the course of this study gave $^{143}Nd/^{144}Nd$ of 0.512105 ± 0.000014 (2 s.d., n=16) and 0.512092 ± 0.000011 (2 s.d., n=11), on the Finnigan MAT261 and Neptune instruments, respectively.

3 – Results

Neodymium concentrations in KZAI-1 sediments (Congo fan) range from 25 to 42 ppm (Table 1). Nd data for other SE Atlantic sediments (from 8 to 28 ppm) and turbidite sands (from 15 to 27 ppm) are lower due to dilution by carbonates and quartz grains, respectively. Hf concentrations in turbidite sands are higher (from 5.2 to 10.3 ppm) than in fine-grained sediments (from 1.9 to 5.0 ppm). Nd isotope compositions of marine muds in the Congo fan (core KZAI-1) are very homogeneous (ε_{Nd} from -15.7 to -16.3), and almost indistinguishable from those for turbidite sands (from -16.0 to -16.9) and associated Fe-oxyhydroxide fractions (from -15.4 to -16.1). In contrast, Hf isotopic compositions for the same mud samples exhibit significant variations (ε_{Hf} from -7.1 to -12.0). The three turbidite sands from the Congo submarine canyon analysed in this study exhibit much lower ε_{Hf} values (from -27.2 to -31.6). Interestingly, the leached Fe-oxide components are characterized by very radiogenic ε_{Hf} values (from -1.1 to +1.3). The Hf and Nd isotopic compositions for the detrital fractions of other SE Atlantic fine-grained sediments range from ε_{Nd} -13.3 to – 7.7 and from ε_{Hf} -8.3 to -2.4, respectively. Note that two sediment samples from the SE Atlantic exhibit however

much lower isotopic ratios: MD96-2091_2cm (ε_{Nd} = -21.9) and MD96-2098_25 cm (ε_{Hf} = -17.6). For the Angola Basin sample (MD96-2091), the very unradiogenic Nd isotope signature most probably reflects a contribution from material delivered by the nearby Kunene River (Fig. 2).

4 – Discussion

4.1 – Leached Fe-oxide fractions and the 'seawater array'

The ferromanganese oxyhydroxide component dispersed in marine sediments is being increasingly used as an archive of deep-ocean circulation and chemistry (Rutberg et al., 2000; Bayon et al., 2002; Piotrowski et al., 2005; Haley et al., 2008). In the open ocean, Fe-Mn oxyhydroxides precipitate from ambient seawater, typically in the form of coatings around foraminifers and detrital particles. Pre-formed oxides, i.e. oxides formed on the continents and delivered to the ocean via aeolian or riverine transport, may also represent an important fraction of the leached Fe-Mn oxide component in deep-sea sediments. Iron-manganese hydroxides are an important weathering product in continental soils, most notably in tropical areas where intense chemical weathering can lead to the formation of laterites and other iron-rich deposits. When they form in soils and/or river waters, those 'pre-formed' Fe-oxides incorporate dissolved trace elements (such as Nd, Pb, Hf) whose isotopic composition can yield important information on chemical weathering conditions. Based on the analysis of a single sediment sample, Bayon et al. (2004) suggested that Fe-oxides leached from Congo fan sediments could correspond to such pre-formed continental oxides. Clearly, this is further confirmed here by the evidence that all leached Fe-oxide fractions exhibit Nd isotopic compositions (ε_{Nd} ~ -16; Table 1) very distinct from the expected seawater ε_{Nd} signature at the studied location and water depth (ε_{Nd} ~ -8 for Antarctic Intermediate waters in the SE Atlantic Ocean; Jeandel, 1993).

It might be argued that this difference relates to the mobility of Nd in the sediments subsequent to their deposition. However, the Nd isotope ratios for those 'pre-formed' Fe-hydroxide components are almost identical to those for detrital sediments. This is consistent with the observation that the dissolved and suspended loads of rivers generally exhibit similar Nd isotopic compositions (e.g. Goldstein and Jacobsen, 1987), reflecting the absence of

233 significant Sm-Nd isotope fractionation during weathering processes (Nesbitt and Markovics,
234 1997; Öhlander et al., 2000; Andersson et al., 2001). In contrast, the Hf isotopic
235 compositions for leached Fe-Mn hydroxide fractions of our Congo fan samples are
236 completely different (more radiogenic) from those measured in associated detrital sediments.
237 This is consistent with the hypothesis that chemical weathering leads to the preferential
238 dissolution of minerals having high ε_{Hf} values (Piotrowski et al., 2000; van de Flierdt et al.,
239 2002), in accord with evidence from river data and leaching experiments (Bayon et al., 2006).
240 The range of ε_{Hf} values in Congo fan oxide fractions (from -1.1 to +1.3) is relatively small,
241 compared to that measured in rivers from the Moselle basin in NE France (from -13.9 to -0.6;
242 Bayon et al., 2006). The Congo River watershed is much larger (about 140 times) than the
243 Moselle basin, draining a much wider range of lithologies. The Central Plain of the Congo
244 Basin consists of Mesozoic and Cenozoic sedimentary rocks (sand, sandstones, red argillites),
245 bordered on the North and the East by Precambrian basement rocks (mainly crystalline and
246 metamorphic rocks; Fig. 1). To some extent, the Congo Basin can be considered as a
247 representative portion of the upper continental crust (UCC). Hence, it is likely that the
248 weathering signal recorded by Fe-hydroxides in Congo fan sediments is more homogeneous,
249 and certainly more representative of continental-scale chemical weathering than that provided
250 by rivers draining small monolithological watersheds (such as the Moselle basin).
251
252 Interestingly, the Hf-Nd isotope data for leached Fe-oxyhydroxide fractions plot on an
253 extension of the seawater array in the ε_{Hf} vs. ε_{Nd} diagram (Fig. 2). The Congo fan data plot on
254 the unradiogenic side of the array defined by deep-sea Fe-Mn crusts and nodules. Although
255 previous studies have clearly shown that the seawater array is a consequence of the mixing
256 between Atlantic waters characterized by low ε_{Hf} and ε_{Nd} values and Pacific waters with
257 radiogenic (high) isotope signatures (Albarède et al., 1998; van de Flierdt et al., 2004), the
258 source of dissolved Hf in the ocean (hydrothermal vs. continental) has remained controversial.
259 Here, the observation that continental Fe-oxides formed in the Congo drainage basin align
260 perfectly on the seawater array provides further support for the hypothesis that the ocean Hf
261 budget is dominated by continental inputs (Bayon et al., 2006; van de Flierdt et al., 2007). As
262 proposed in those previous studies, these new data suggest that ocean water masses mainly
263 acquire their Hf isotope signature from the weathering of surrounding terranes (e.g. old
264 cratonic areas for North Atlantic deep waters; the young volcanic circum-Pacific belt for
265 Pacific deep waters). Further work would, however, be required to assess whether submarine

hydrothermal systems may contribute, at least to some extent, to the dissolved Hf ocean budget.

The evidence that Congo fan Fe-Mn oxides plot apart from the field of ε_{Nd} and ε_{Hf} data defined by marine Fe-Mn crusts and nodules most probably reflects a sampling issue. To date, the only available information on the Hf isotopic composition of seawater has been derived from the analysis of deep-sea Fe-Mn precipitates, which exhibit a range of Nd isotopic compositions (from ε_{Nd} ~ -13 to -2) that does not cover the full range of ε_{Nd} values measured in seawater. For example, the Labrador Sea, in the northwest Atlantic Ocean, and the Baltic Sea are both characterized by much lower Nd isotopic signatures (ε_{Nd} ~ -24; Andersson et al., 1992; Lacan, 2002). Most likely, therefore, it is expected that the distribution of ε_{Nd} and ε_{Hf} values in the ocean defines a seawater array that extends beyond the field defined by ferromanganese crusts, towards more unradiogenic values. This should be confirmed soon with the first direct acquisition of Hf isotope data in seawater samples (unpublished data from Zimmermann et al., 2003; Rickli et al., 2007).

4.2 – Marine muds and the 'zircon-free sediment array'

Neodymium isotopes are excellent tracers of the geographical provenance of marine sediments because, unlike many other radiogenic isotope systems (e.g. Sr, Pb, Hf), they are not significantly fractionated during continental weathering and sediment transport. In this study, all the fine-grained sediments from the Congo fan area display very similar Nd isotopic compositions, which suggests that they are derived from a common source. As discussed earlier, the Congo basin integrates the lithological and chemical diversity of the UCC. Hence, it is likely that the Nd isotopic composition of clays delivered by the Congo River has remained quite constant, at least over the period of time encompassed by the studied core KZAI-1 (i.e. ~40,000 years; F. Jansen, pers. comm.).

By contrast, the data indicate that the Hf isotopic composition of suspended material transported by the Congo River has varied significantly during the Late Quaternary period. Grain-size variations, associated with changes in the relative proportions of mineral phases having distinct Hf isotope signatures, cannot account for the large ε_{Hf} range observed in Congo fan clays because of grain-size homogeneity in the studied sediments. Instead, it seems most likely that the Hf isotopic variations in fine-grained sediments from the Congo fan are due to variations in the congruence of silicate weathering. This hypothesis can be verified by comparing ε_{Hf} to Al/K ratios for the Congo fan sediments (Fig. 3). Variations of

Al/K in Equatorial Atlantic sediment cores provide an index for the intensity of chemical weathering in Central Africa through time (Schneider et al., 1997; Zabel et al., 2001). Aluminium is one of the least mobile elements during continental weathering, being incorporated into secondary clay minerals such as kaolinite, in marked contrast with K which is highly mobile and typically depleted in soils. High Al/K ratios in Congo fan sediments are therefore considered to be indicative of intense chemical weathering. The Al/K ratio correlates very well with ε_{Hf} values in fine-grained Congo fan sediments (Fig. 3). Sediments with the highest Al/K ratios are also characterized by the most radiogenic Hf isotope values. This suggests that intensification of chemical weathering in Central Africa during the Late Quaternary period led to the dissolution of a more radiogenic fraction of Hf and, consequently, to the formation of secondary clay minerals having higher ε_{Hf} values. Interestingly, the best-fit regression line passes through a theoretical unweathered rock endmember for the Congo Basin (Fig. 3). This adds further support for a direct relationship between the Hf isotopic composition of secondary clay minerals and intensity of chemical weathering. Finally, these Hf-Nd data for Congo fan sediments have important implications on how weathering in Central Africa has been linked to climate change during the Late Quaternary, but these will be discussed elsewhere.

The Hf-Nd isotope data for the Congo fan clays and other studied SE Atlantic sediments are reported in the ε_{Hf} vs. ε_{Nd} diagram, together with existing literature data (Fig. 2). With the exception of sample MD96-2098_25cm, our data for marine muds plot well above the 'igneous rock array'. The 'igneous rock array' is defined here as the correlation for *unweathered* whole-rock data, hence excluding all sedimentary rocks (Fig. 2). Note that the trend for the 'igneous rock array' ($\varepsilon_{Hf} = 1.37\varepsilon_{Nd} + 2.89$) is very similar to that for the 'terrestrial array' ($\varepsilon_{Hf} = 1.36\varepsilon_{Nd} + 2.95$; Vervoort et al., 1999). All Hf-Nd data available to date for fine-grained sediments (Vervoort et al., 1999; Pettke et al., 2002; Vlastelic et al., 2005; Prytulac et al., 2006; van de Flierdt et al., 2007), including data from this study, are distributed along a shallower and more diffuse array. As discussed above, the Hf isotopic composition of clays is highly sensitive to chemical weathering intensity. Hence, the large scatter in the mud data observed in the ε_{Hf} vs. ε_{Nd} diagram could be explained by the fact that sediments can form under a large range of chemical weathering conditions, depending on their geographical provenance. Another possibility is that some of those fine-grained sediments actually contain a minor portion of zircon, which would explain some of the lowest

ε_{Hf} values observed. This may be the case, for example, for sample MD96-2098_25cm (with a very low ε_{Hf} value; Table1), but also for sediment samples from the Southern Ocean, which are known to contain a fraction of ice-rafted debris that could include zircon grains (Vlastelic et al., 2005; van de Flierdt et al., 2007; Roy et al., 2008). When excluding those latter samples, plus two Paleozoic shale samples characterized by highly negative initial ε_{Hf} values (analysed by Vervoort et al., 1999), fine-grained sediments define a shallower array with an equation of $\varepsilon_{Hf} = 0.91\ \varepsilon_{Nd} + 3.10$, which can be defined as the 'zircon-free sediment array'.

4.3 – Turbiditic sands and the 'zircon-bearing' sediment array

The high Hf concentrations (from 5.2 to 10.3 ppm) and very low ε_{Hf} values (lower than -27) measured in the three turbiditic sands from the Congo submarine canyon indicate the presence of zircon in those samples. Vervoort et al. (1999) showed previously that zircon sorting in coarse-grained sediments results in a significant decoupling between Lu-Hf and Sm-Nd isotope systems. This is clearly illustrated here by the evidence that sands and muds from the same sedimentary system (i.e. the Congo basin) exhibit distinct Hf isotopic signatures, but almost identical Nd isotope ratios. As mentioned previously by Vervoort et al. (1999), a consequence of this zircon effect is that zircon-bearing sediments plot generally below the 'terrestrial array' in the ε_{Hf} vs. ε_{Nd} diagram (i.e. have lower initial ε_{Hf} values for a given ε_{Nd} value), along a much steeper trend toward more negative ε_{Hf} values ($\varepsilon_{Hf} = 1.80\ \varepsilon_{Nd} + 2.35$; Fig. 2).

4.4 – Constraints on global silicate weathering

As discussed above, incongruent dissolution of silicate rocks during chemical weathering in Central Africa leads to products of erosion having very distinctive ε_{Hf} signatures. All continental Fe-Mn hydroxides, clays and turbidite sands from those SE Atlantic sediments align remarkably well on the global arrays identified in the ε_{Hf} vs. ε_{Nd} diagram for seawater, zircon-free and zircon-bearing sediments, respectively. In which case, these data suggest that the Hf-Nd arrays could result entirely from crustal weathering (i.e. with little or no hydrothermal input). Below, this hypothesis is assessed using a simple weathering model of the continental crust. A model is used in which chemical weathering of pristine portions of the upper continental crust (UCC) produces a dissolved fraction, secondary clay minerals and residual coarse-grained sediments (Fig. 4). By considering the Hf-Nd arrays for seawater, igneous rocks and zircon-bearing sediments, and making reasonable assumptions about the

mean Hf concentration for each reservoir (see Fig. 4 caption), it is possible to calculate the ε_{Hf} signature of secondary clay minerals for any given ε_{Nd}, simply by using mass balance considerations (Fig. 4a). It is assumed here that the 'seawater array' is generated solely by chemical weathering of continental rocks. Using mass balance equations, our estimated Hf concentrations (i.e. 5.8 ppm for UCC; 4.0 ± 1.3 ppm for the fraction of rock dissolved by chemical weathering and for fine-grained sediments; 8.9 ± 3.2 ppm for residual sands; Fig. 4a) can be used to calculate the fraction of residual sands left after chemical weathering. This leads to an estimation of ~40% of coarse-grained sediments being generated by chemical weathering of UCC.

Then, a Monte Carlo procedure is used to generate simulations of the weathering of the upper continental crust, and to calculate corresponding ε_{Hf} values for secondary clay minerals. The uncertainties on estimated Hf concentrations are taken into account in the weathering model. Results are expressed as density fields in the ε_{Hf} vs. ε_{Nd} diagram (Fig. 4b). For a proportion of residual sands of 40±10%, the density fields of modeled ε_{Hf} - ε_{Nd} data (acquired during 50,000 Monte Carlo simulation runs) fall on the array defined above for fine-grained sediments, overlapping remarkably well the range of available Hf-Nd isotope data for sediments (Fig. 4b). Previous studies have already shown that deep-sea sediments commonly exhibit higher Hf ratios than other rocks at a given Nd ratio, but the significance of this offset was unclear (Pettke et al., 2002; Chauvel et al., 2008). Chauvel et al. (2008) suggested that high ε_{Hf} values for sediments may reflect the incorporation of radiogenic (high ε_{Hf}) seawater-derived material (e.g. Fe-Mn oxyhydroxides) in marine sediments during post-depositional redistribution processes. Instead, our modeling shows that the entire distribution of Hf-Nd isotope ratios in fine-grained sediments can be generated solely by chemical weathering. Hence, the important result in the context of this discussion is that it is possible to reconcile the Hf-Nd isotope variability observed in igneous rocks, marine precipitates, fine-grained sediments and sands, with a simple weathering model of the upper continental crust.

5 – Concluding remarks

The incongruent dissolution of silicate rocks during chemical weathering leads to products of erosion having very distinctive but systematic ε_{Hf} signatures. Taken alone, Hf isotopes in sediment records cannot distinguish changes due to variations in chemical weathering from those caused by variations in sediment sources. But by combining Lu-Hf with the Sm-Nd isotope system, which exhibit a globally similar behavior but is much less prone to

fractionation during silicate weathering, it becomes possible to discriminate between both weathering and provenance signals. Hence, Hf-Nd isotope analyses of sediments preserved in the geological record provide a powerful tool, which can be used to trace the evolution of continental weathering through time. The Hf-Nd decoupling during silicate weathering leads to distinct arrays in the ε_{Hf} vs. ε_{Nd} diagram: a 'zircon-bearing sediment array', a diffuse 'zircon-free sediment array', and generates most probably the 'seawater array' defined by marine ferromanganese precipitates. Further work is now required to better constrain the significance of ε_{Hf} in fine-grained sediments. Additional analyses of modern river-borne sediments from various locations should help in determining the factors (e.g. lithology, temperature, runoff, basin elevation) that control, for any given ε_{Nd}, the extent to which ε_{Hf} of fine sediments deviates from the 'igneous rock array'.

Acknowledgements

We gratefully acknowledge P. Bertrand and J. Giraudeau (University of Bordeaux) for giving us access to IMAGES core sediments. Sediment cores from the Congo Fan area were collected as part of the ZaiAngo project, funded by IFREMER and TOTAL. C. Hémond and M. Benoit from the Institut Universitaire Européen de la Mer (Brest, France) are thanked for the access to the Element2 and technical assistance. We are grateful to A. Milton, N. Rogers and A. Cohen for operating the ICP-MS instruments at NOCS and The Open University, respectively. L. Dosso is thanked for assistance on the Finnigan MAT261 at IFREMER. Three anonymous reviewers are acknowledged for providing detailed reviews, which improved significantly our manuscript. Research was funded by an Open University Post-Doctoral Fellowship (GB), through the program 'Ressources minérales et énergétiques, processus sédimentaires et impact sur les écosystèmes' at IFREMER, and via EU-FEDER funding (acquisition of the MC-ICPMS instrument at IFREMER). This paper is dedicated to the memory of our IFREMER colleague Bruno Savoye, who had been the head of the ZaiAngo project.

426 **References**

427 Albarède, F., Simonetti, A.,Vervoort, J.D., Blichert-Toft, J., Abouchami,W., 1998. A Hf–Nd
428 isotopic correlation in ferromanganese nodules. Geophys. Res. Lett. 25, 3895–3898.

429 Allègre, C.J., Dupré, B., Négrel, P., Gaillardet, J., 1996. Sr-Nd-Pb isotope systematics in
430 Amazon and Congo River systems: Constraints about erosion processes. Chem. Geol. 131,
431 93-112.

432 Andersson, P.S., Wasserburg, G.J., Ingri, J., 1992. The sources and transport of Sr and Nd
433 isotopes in the Baltic Sea. Earth Planet. Sci. Lett. 113, 459-472.

434 Andersson, P.S., Dahlqvist, R., Ingri, J., Gustafsson, Ö., 2001. The isotopic composition of
435 Nd in a boreal river: A reflection of selective weathering and colloidal transport.
436 Geochim. Cosmochim. Acta 65, 521-527.

437 Babonneau, N., Savoye, B., Cremer, M., Klein, B., 2002. Morphology and architecture of the
438 present canyon and channel system of the Zaire deep-sea fan. Mar. Petrol. Geol. 19, 445-
439 467.

440 Bau, M., Koschinsky, A., 2006. Hafnium and neodymium isotopes in seawater and in
441 ferromanganese crusts: the “element” perspective. Earth Planet. Sci. Lett. 241, 952–961.

442 Bayon, G., German, C.R., Boella, R.M. Milton, J.A. Taylor, R.N. Nesbitt, R.W., 2002. Sr and
443 Nd isotope analyses in paleoceanography: the separation of both detrital and Fe–Mn
444 fractions from marine sediments by sequential leaching. Chem. Geol. 187, 179–199.

445 Bayon, G., German, C.R., Nesbitt, R.W., Bertrand, P., Schneider, R., 2003. Increased input of
446 circumpolar deep water-borne detritus to the glacial SE Atlantic Ocean. Geochem.
447 Geophys. Geosys. 4, 1025.

448 Bayon, G., German, C.R., Burton, K.W., Nesbitt, R.W., Rogers, N., 2004. Sedimentary Fe–
449 Mn oxyhydroxides as paleoceanographic archives and the role of aeolian flux in regulating
450 oceanic dissolved REE. Earth Planet. Sci. Lett. 224, 477–492.

451 Bayon, G., Vigier, N., Burton, K.W., Brenot, A., Carignan, J., Etoubleau, J., Chu, N.-C.,
452 2006. The control of weathering processes on riverine and seawater hafnium isotope ratios.
453 Geology 34, 433–436.

454 Bayon, G., Barrat, J.-A., Etoubleau, J., Benoit, M., Bollinger, C., Révillon, S., 2008.
455 Determination of rare earth elements, Sc, Y, Zr, Ba, Hf and Th in geological samples by
456 ICP-MS after Tm addition and alkaline fusion. Geostand. Geoanal. Res., in press.

457 Bentahila, Y., Hebrard, O., Ben Othman, D., Luck, J.-M., Seranne, M., Lopez, M., 2006.
458 Gulf of Guinea continental slope and Congo (Zaire) deep-sea fan: Sr-Pb isotopic
459 constraints on sediments provenance from ZaiAngo cores. Mar. Geol. 226, 323-332.

460 Berner, R.A., Lassaga, A.C., Garrels, R.M., 1983. The carbonate-silicate geochemical cycle
461 and its effect on atmospheric carbon dioxide over the past 100 million years. Am. J. Sci.
462 284, 641-683.
463 Bertrand, P., Pedersen, T.F., Schneider, R., Shimmield, G., Vergès, E., Disnar, J.R., Massias,
464 D., Villanueva, J., Tribovillard, N., Huc, A.Y., Giraud, X., Pierre, C., M.Th, Vénec-Peyré,
465 2003. Organic rich sediments in deep-sea ventilated environments: relationship to climate
466 change, sea-level, and trophic changes, J. Geophys. Res. 108, doi:2000JC000327.
467 Chauvel, C., Lewin, E., Carpentier, M., Arndt, N.T., Marini, J.-C., 2008. Role of recycled
468 oceanic basalt and sediment in generating the Hf-Nd mantle array. Nature Geosci. 1, 64-
469 67.
470 Chu, N.-C., Taylor, R.N., Chavagnac, V., Nesbitt, R.W., Boella, R.M., Milton, J.A., German,
471 C.R., Bayon, G., Burton, K.W., 2002. Hafnium isotope ratio analysis using multi-
472 collector inductively coupled plasma mass spectrometry: an evaluation of isobaric
473 interference corrections. J. Anal. Atom. Spec. 17, 1567-1574.
474 Clift, P.D., 2005. Reorganization of the western Himalayan river system after five million
475 years ago. Nature 438, 1001-1003.
476 Clift, P.D., Giosan, L., BIusztajn, J., Campbell, I.H., Allen, C., Pringle, M., Tabrez, A.R.,
477 Danish, M., Rabbani, M.M., Alizai, A., Carter, A., Lueckge, A., 2008. Holocene erosion
478 of the Lesser Himalaya triggered by intensified summer monsoon. Geology 36, 79-82.
479 Edmond, J.M., 1992. Himalayan tectonics, weathering processes and the strontium isotope
480 record in marine limestones. Science 258, 1594-1597.
481 Erlank, A.J., Smith, H.S., Marchant, J.W., Cardoso, M.P., Ahrens, L.H., 1978. Hafnium, in:
482 Wedepohl, K.H. (Ed.), Handbook of Geochemistry. Springer-Verlag, Berlin, Heidelberg,
483 New York, pp. 72B– 72O.
484 Foster, G.L., Vance, D., 2006. Negligible glacial-interglacial variation in continental chemical
485 weathering rates. Nature 444, 918-921.
486 Godfrey, L.V., Lee, D.-C., Sangrey,W.F., Halliday, A.N., Salters, V.J.M., Hein, J.R., White,
487 W.M., 1997. The Hf isotopic composition of ferromanganese nodules and crusts and
488 hydrothermal manganese deposits: implications for seawater Hf. Earth Planet. Sci. Lett.
489 151, 91–105.
490 Goldstein, S.L., O'Nions, R.K., Hamilton, P.J., 1984. A Sm–Nd isotopic study of atmospheric
491 dusts and particulates from major river systems. Earth Planet. Sci. Lett. 70, 221–236.

492 Goldstein, S.J., Jacobsen, S.B., 1987. The Nd and Sr isotopic systematics of river-water
493 dissolved material: implications for the sources of Nd and Sr in seawater. Chem. Geol.
494 66, 245-272.
495 Haley, B.A., Frank, M., Spielhagen, R.F., Eisenhauer, A., 2008. Influence of brine formation
496 on Arctic Ocean circulation over the past 15 million years. Nature Geosci. 1, 68-72.
497 Hoskin, P.W.O., Schaltegger, U., 2003. The composition of zircon and igneous and
498 metamorphic petrogenesis, in: Hanchar, J.M., Hoskin, P.W.O. (Eds.), Reviews in
499 Mineralogy and Geochemistry — Zircon. Mineralogical Society of America and
500 Geochemical Society, Washington D.C, pp. 27–62.
501 Huh, Y., Chan, L.H., Chadwick, O.A., 2004. Behavior of lithium and its isotopes during
502 weathering of Hawaiian basalt. Geochem. Geophys. Geosys. 5, Q09002.
503 Jeandel, C., 1993. Concentration and isotopic composition of Nd in the South Atlantic Ocean.
504 Earth Planet. Sci. Lett. 117, 581–591.
505 Jung, S.J.A., Davies, G.R., Ganssen, G.M., Kroon, D., 2004. Stepwise Holocene aridification
506 in the NE Africa deduced from dust-borne radiogenic isotope records. Earth Planet. Sci.
507 Lett. 221, 27–37.
508 Lacan, F., 2002. Masses d'eau des Mers Nordiques et de l'Atlantique Subarctique tracées par
509 les isotopes du néodyme. PhD Thesis. Toulouse III University, France.
510 Nesbitt, H.W., Markovics, G., 1997. Weathering of granodioritic crust, long-term storage of
511 elements in weathering profiles, and petrogenesis of siliciclastic sediments. Geochim.
512 Cosmochim. Acta 61, 1653-1670.
513 Öhlander, B., Ingri, J., Land, M., Schöberg, H., 2000. Change of Sm–Nd composition during
514 weathering of till. Geochim. Cosmochim. Acta 64, 813-820.
515 Patchett, P.J., White, W.M., Feldmann, H., Kielinczuk, S., Hofmann, A.W., 1984.
516 Hafnium/rare earth element fractionation in the sedimentary system and crustal recycling
517 into the Earth's mantle. Earth Planet. Sci. Lett. 69, 365–378.
518 Pettke, T., Lee, D.C., Halliday, A.N., Rea, D.K., 2002. Radiogenic Hf isotopic compositions
519 of continental eolian dust from Asia, its variability and its implications for seawater Hf.
520 Earth Planet. Sci. Lett. 202, 453–464.
521 Pichevin, L., Bertrand, P., Boussafir, M., Disnar, J.-R., 2004. Organic matter accumulation
522 and preservation controls in a deep sea modern environment: an example from Namibian
523 slope sediments. Org. Geochem. 3, 543–559.

524 Pichevin, L., Cremer, M., Giraudeau, J. Bertrand, P., 2005. A 190 ky record of lithogenic
525 grain-size on the Namibian slope: forging a tight link between past wind-strength and
526 coastal upwelling dynamics. Mar. Geol. 218, 81–96.
527 Piotrowski, A.M., Lee, D.-C., Christensen, J.N., Burton, K.W., Halliday, A.N., Hein, J.R.,
528 Günther, D., 2000. Changes in erosion and ocean circulation recorded in the Hf isotopic
529 compositions of North Atlantic and Indian Ocean ferromanganese crusts. Earth Planet. Sci.
530 Lett. 181, 315–325.
531 Piotrowski, A.M., Goldstein, S.L., Hemming, S.R., Fairbanks, R.G., 2005. Temporal
532 relationships of carbon cycling and ocean circulation at glacial boundaries. Science 307,
533 1933–1938.
534 Prytulak, J., Vervoort, J.D., Plank, T., Yu, C., 2006. Astoria Fan sediments, DSDP site 174,
535 Cascadia Basin: Hf–Nd–Pb constraints on provenance and outburst flooding. Chem.
536 Geol. 233, 276–292.
537 Raymo, M.E., Ruddiman, W.F., 1992. Tectonic forcing of Late Cenozoic climate. Nature 359,
538 117-122.
539 Raymo, M.E., Ruddiman, W.F., Froelich, P.N., 1988. Influence of late Cenozoic mountain
540 building on ocean geochemical cycles. Geology 16, 649-653.
541 Ravizza, G., Peucker-Ehrenbrink, B., 2003. Chemostratigraphic Evidence of Deccan
542 Volcanism from the Marine Osmium Isotope Record. Science 302, 1392-1395.
543 Rickli, J., Frank, M., Halliday, A.N., 2007. Hafnium and neodymium isotopes in Atlantic
544 ocean waters. Geochim. Cosmochim. Acta 71, A841-A841.
545 Roy, M., van de Flierdt, T., Hemming, S.R., Goldstein, S.L., under revision. Sm–Nd isotopes
546 and 40Ar/39Ar ages of proximal circum- Antarctic sediments: reflections of Antarctica's
547 geological history. Chem. Geol.
548 Rutberg, R.L., Hemming, S.R., Goldstein, S.L., 2000. Reduced North Atlantic Deep Water
549 flux to the glacial Southern Ocean inferred from neodymium isotope ratios. Nature 405,
550 935–938.
551 Savoye, B., Cochonat, P., Apprioual, R., Bain, O., Baltzer, A., Bellec, V., Beuzart, P.,
552 Bourillet, J.F., Cagna, R., Cremer, M., Crusson, A., Dennielou, B., Diebler, D., Droz, L.,
553 Ennes, J.C., Floch, G., Foucher, J.P., Guiomar, M., Harmegnies, F., Kerbrat, R., Klein, B.,
554 Khun, H., Landure, J.Y., Lasnier, C., Le Drezen, E., Le Formal, J.P., Lopez, M., Loubrieu,
555 B., Marsset, T., Migeon, S., Normand, A., Nouze, H., Ondreas, H., Pelleau, P., Saget, P.,
556 Seranne, M., Sibuet, J.C., Tofani, R., Voisset, M., 2000. Structure et évolution récente de

l'éventail turbiditique du Zaïre: Premier résultats scientifiques des missions d'exploration ZaiAngo 1 and 2 (Marge Congo–Angola). CRAS 331, 211–220.

Schneider, R., Price, B., Muller, P., Kroon, D., Alexander, I., 1997. Monsoon-related variations in Zaire (Congo) sediment load and influence of fluvial silicate supply on marine productivity in the east equatorial Atlantic during the last 200,000 years, Paleoceanography 12, 463–481.

Soederlund, U., Patchett, P.J., Vervoort, J.D., Isachsen, C.E., 2004. The 176Lu decay constant determined by Lu–Hf and U–Pb isotope systematics of Precambrian mafic intrusions. Earth Planet. Sci. Lett. 219, 311–324.

Taylor, S.R., McLennan, S.M., 1985. The Continental Crust: its Composition and Evolution. Blackwell Scientific Publications, Oxford.

van de Flierdt, T., Frank, M., Lee, D.-C., Halliday, A.N., 2002. Glacial weathering and the hafnium isotope composition of seawater. Earth Planet. Sci. Lett. 201, 639–647.

van de Flierdt, T., Frank, M., Lee, D.-C., Halliday, A.N., Reynolds, B.C., Hein, J.R., 2004. New constraints on the sources and behavior of neodymium and hafnium in seawater from Pacific Ocean ferromanganese crusts. Geochim. Cosmochim. Acta 68, 3827–3843.

van de Flierdt, T., Goldstein, S.L., Hemming, S.R., Roy, M., Frank, M., Halliday, A.N., 2007. Global Neodymium-Hafnium isotope systematic - Revisited. Earth Planet. Sci. Lett. 259, 432–441.

Vervoort, J.D., Patchett, P.J., Blichert-Toft, J., Albarède, F., 1999. Relationships between Lu–Hf and Sm–Nd isotopic systems in the global sedimentary system. Earth Planet. Sci. Lett. 168, 79–99.

Vigier, N., Decarreau, A., Millot, R., Carignan, J., Petit, S., France-Lanord, C., 2008. Quantifying Li isotope fractionation during smectite formation and implications for the Li cycle. Geochim. Cosmochim. Acta 72, 780-792.

Vlastelic, I., Carpentier, M., Lewin, E., 2005. Miocene climate change recorded in the chemical and isotopic (Pb, Nd, Hf) signature of Southern Ocean sediments. Geochem. Geophys. Geosys. 6, Q03003.

Walker, J.C.G., Hays, P.B., Kasting, J.F., 1981. A negative feedback mechanism for the long-term stabilization of Earth's surface temperature. J. Geophys. Res. 86, 9776-9782.

White, W.M., Patchett, J., Ben Othman, D., 1986. Hf isotope ratios of marine sediments and Mn nodules: evidence for a mantle source of Hf in seawater. Earth Planet. Sci. Lett. 79, 46–54.

590 Zabel, M., Schneider, R.R., Wagner, T., Adegbie, A.T., de Vries, U., Kolonic, S., 2001. Late
591 Quaternary climate changes in central Africa as inferred from terrigenous input to the
592 Niger fan. Quat. Res. 56, 207-217.
593 Zimmermann, B.E., Lee D., Porcelli D., Frank, M., Halliday, A.N., Andersson, P.S.,
594 Baskaran, M., 2003. The isotopic composition of Hafnium in seawater: first results from
595 the Artic Ocean. Eos Trans. AGU 84, Ocean Sci. Meet. Supll. Abstr. OS32K-09.
596
597

598 **Figure captions**

599

600 **Figure 1**. **South Atlantic area showing sample locations and simplified geological map of**
601 **the Congo River Basin**. The Congo fan is incised by a large submarine canyon, which
602 ensures an efficient transfer of coarse-grained sediments from the river estuary to the deep
603 basin (Savoye et al., 2000; Babonneau et al., 2002). The Cape Basin cores are located
604 directly under the trajectory of southeast trade winds, and hence may contain a significant
605 fraction of aeolian dust blown from the nearby Namib Desert (Bayon et al., 2003; Pichevin et
606 al., 2005). Other sediment sources in the deep SE Atlantic include clays delivered from
607 tropical rivers, transported south by north Atlantic deep waters, and material from the
608 southwest Atlantic province advected northward by circumpolar deep waters (Bayon et al.,
609 2003). The simplified geological map of the Congo Basin is modified from Bentahila et al.
610 (2006). The Central Plain of the Congo Basin consists of Mesozoic and Cenozoic
611 sedimentary rocks (sand, sandstones, red argillites), bordered on the North and the East by
612 Precambrian basement rocks.

613

614 **Figure 2**. **Initial ε_{Hf} and ε_{Nd} values for marine sediments and other sedimentary rocks,**
615 **marine precipitates and igneous rocks**. Data from this study correspond to SE Atlantic fine
616 sediments (blue filled diamonds), Congo turbidite sands (red filled triangles) and Congo Fe-
617 hydroxides (green filled circles). Data for other marine sediments and fine-grained
618 sedimentary rocks are from Vervoort et al. (1999), Pettke et al. (2002), Vlastelic et al. (2005),
619 Prytulac et al. (2006) and van de Flierdt et al. (2007). Fine-grained sediments (blue field)
620 define a diffuse shallow array with an equation of $\varepsilon_{Hf} = 0.91\ \varepsilon_{Nd} + 3.10$, which is referred to as
621 the 'zircon-free sediment array'. Data for coarse-grained sediments come primarily from
622 Vervoort et al.'s study, which includes Hf-Nd isotope analysis of sands, sandstones,
623 greywacke, siltstones and quartzite. A few samples collected from a turbidite-rich
624 sedimentary sequence (Astoria fan, NW coast of USA; Prytulak et al., 2006) were also
625 considered as coarse-grained sediments on the basis of their high Hf contents (i.e. samples
626 having Hf concentrations higher than 5.3 ppm), suggesting the presence of zircon in those
627 samples. Coarse-grained sediments (orange field) plot along a steep array, defined as the
628 'zircon-bearing sediment array' ($\varepsilon_{Hf} = 1.80\ \varepsilon_{Nd} + 2.35$). Background data for igneous rocks
629 and marine Fe-Mn precipitates are from the literature. The 'igneous rock array' ($\varepsilon_{Hf} = 1.37\varepsilon_{Nd}$
630 + 2.89) is the correlation for unweathered whole-rock data, hence excluding sedimentary

631 rocks. The 'seawater array' is the correlation for marine Fe-Mn precipitates ($\varepsilon_{Hf} = 0.39\varepsilon_{Nd} +$
632 6.2).
633
634 **Figure 3**. **Relationship between ε_{Hf} and Al/K in Congo fine sediments**. Al/K ratios in
635 Equatorial Atlantic sediment cores provide an index for the intensity of chemical weathering
636 in Central Africa through time (Schneider et al., 1997; Zabel et al., 2001). The theoretical
637 unweathered rock endmember for the Congo Basin is defined using 1) the average ε_{Nd} value
638 for Congo River suspended material (-16; Goldstein et al., 1984, Allègre et al., 1996, This
639 study) and ε_{Hf} inferred graphically from the 'terrestrial array' (Vervoort et al., 1999); and 2)
640 estimated Al and K values for the upper continental crust (Taylor and McLennan, 1985).
641
642 **Figure 4**. **Weathering model of the continental crust. (a)** Mass balance equation for the
643 chemical weathering of pristine portions of the upper continental crust (UCC), which
644 produces a dissolved fraction, secondary clay minerals and residual coarse-grained sediments.
645 $\varepsilon_{Hf\ PRIS}$ and $[Hf]_{PRIS}$ are the Hf isotopic composition and concentration of the unweathered
646 upper continental crust, respectively. $\varepsilon_{Hf\ DISS}$ and $[Hf]_{DISS}$ are the Hf isotopic composition and
647 concentration of the fraction of unweathered rock dissolved by chemical weathering, from
648 which Fe-oxide precipitates may form (either in soils, river waters or seawater). $\varepsilon_{Hf\ CLAY}$, ε_{Hf}
649 $_{SAND}$ and $[Hf]_{CLAY}$, $[Hf]_{SAND}$ are the Hf isotopic compositions and concentrations of secondary
650 clay minerals and residual coarse-grained sediments, respectively. *x*, *y* and *z* represent the
651 fractions of the upper continental crust that have been i) dissolved, ii) incorporated into
652 secondary clay minerals, and iii) left as residual sands during chemical weathering,
653 respectively. The average Hf concentration of the residual sands is difficult to evaluate
654 because zircon sorting during sedimentary transport causes a very large scatter in the [Hf]
655 data of coarse-grained sedimentary rocks (e.g. from ~ 0.6 to 35 ppm; Vervoort et al., 1999).
656 In continental rocks, a major fraction of Hf is hosted in zircon (i.e. zircon contains up to 6%wt
657 of Hf; Erlank et al., 1978; Hoskin and Schaltegger, 2003). As a consequence, in an ideally
658 closed system (i.e. not affected by sediment transport), the [Hf] content of residual zircon-
659 bearing sands is expected to be higher than the bulk UCC Hf concentration (5.8 ppm; Taylor
660 and McLennan, 1985). To estimate the average [Hf] concentration of residual sands, we
661 consider therefore only coarse-grained sedimentary rocks having [Hf] concentrations higher
662 than 5.8 ppm (Table 2). This leads to a mean value of 8.9 ppm, with significant uncertainty
663 however (±3.2 ppm; 1SD, n=22). The Hf concentration of terrigenous fine-grained

664 sedimentary rocks and river suspended particles is much more homogeneous, averaging ~4.0
665 ± 1.3 ppm (1SD; n=135; Table 2). The average Hf concentration of the rock fraction
666 dissolved during chemical weathering (i.e. $[Hf]_{DISS}$; Fig. 4) is difficult to assess, because it
667 cannot be inferred directly from the Hf concentration of river waters or Fe-oxides. Bayon et
668 al. (2006) showed that the Hf isotope composition of river waters is controlled by preferential
669 dissolution of accessory phases (i.e., apatite, sphene, allanite) versus more resistant minerals
670 (e.g., biotite, plagioclase, K-feldspar). Although those minerals are characterized by
671 distinctive Lu/Hf ratios (leading with time and radioactive decay of ^{176}Lu to ^{176}Hf to distinct
672 ε_{Hf} signatures), most of them are characterized globally by ppm levels of hafnium, with the
673 exception of sphene and feldspar, which commonly exhibit higher (>10 ppm) and lower (0.1
674 ppm) Hf contents, respectively. This suggests that the mean Hf concentration of the rock
675 fraction dissolved during chemical weathering may not be significantly different than the
676 average [Hf] value for secondary clay minerals. Although leaching experiments on a wide
677 variety of rock types would be needed to better constrain this value, we assume in our model,
678 to a first approximation, that $[Hf]_{DISS} \approx [Hf]_{CLAY} \sim 4.0 \pm 1.3$ ppm.
679 **(b)** Simulations of the weathering of continental crust and corresponding calculated ε_{Hf} values
680 for secondary clay minerals. The Monte Carlo procedure is used to sample random ε_{Nd} values
681 between -18 and +7, random $[Hf]_{DISS}$, $[Hf]_{CLAY}$ and $[Hf]_{SAND}$ within the range of
682 concentrations given above, and random proportions of sand between 30% and 50%. Hf
683 concentrations were assumed to follow a gaussian distribution. For each simulation, ε_{Hf} for
684 the pristine unweathered rock, dissolved fraction and residual sands were calculated using the
685 arrays defined for marine precipitates (seawater array), igneous rocks and zircon-bearing
686 sediments (see dashed lines). The calculated density field represents the result of modeled ε_{Hf}
687 - ε_{Nd} data acquired during 50,000 simulations. Diamonds correspond to Hf-Nd data for fine-
688 grained sediments, defining the 'zircon-free sediment array' (see bold line). The good overlap
689 between our modeled Hf-Nd data for secondary clays and existing data for fine-grained
690 sediments suggests that the global distribution of Hf-Nd isotope data in marine sediments can
691 be generated by weathering of the continental crust.
692

Table1
Click here to download Table: Table.pdf

Table 1. Hf and Nd isotope compositions of SE Atlantic sediments

Sediment samples (depth in core cm)	Leach/Digestion method	$^{143}Nd/^{144}Nd$ ± 2 se	ε_{Nd}	± 2 sd	[Nd] (ppm)	[Sm] (ppm)	$^{176}Hf/^{177}Hf$ ± 2 se	ε_{Hf}	± 2 sd	[Hf] (ppm)	[Lu] (ppm)
Leached Fe-hydroxide fractions (Congo fan)											
KZAI-01 - 6 cm	HH	0.511813 ± 7	-16.05	± 0.27	-	-	0.282814 ± 12	1.5	± 4.5		
'	0.2M HNO_3	-	-		-	-	0.282808 ± 16	1.3	± 1.6	-	-
KZAI-01 - 41 cm	HH	0.511849 ± 6	-15.35	± 0.27	-	-	-	-		-	-
'	0.2M HNO_3	-	-		-	-	0.282780 ± 11	0.3	± 1.6	-	-
KZAI-01 - 47 cm	HH	0.511830 ± 6	-15.72	± 0.27	-	-	-	-		-	-
'	0.2M HNO_3	-	-		-	-	0.282785 ± 17	0.4	± 1.6	-	-
KZAI-01 - 241 cm	HH	0.511811 ± 6	-16.09	± 0.27	-	-	0.282780 ± 82	0.3	± 2.9		
'	0.2M HNO_3	-	-		-	-	0.282789 ± 12	0.6	± 1.6	-	-
KZAI-01 - 341 cm	HH	-	-		-	-	-	-		-	-
'	0.2M HNO_3	-	-		-	-	0.282764 ± 15	-0.3	± 1.6	-	-
KZAI-01 - 421 cm	HH	0.511827 ± 6	-15.78	± 0.27	-	-	0.282667 ± 94	-3.7	± 3.3		
'	0.2M HNO_3	-	-		-	-	0.282787 ± 19	0.5	± 1.6	-	-
KZAI-01 - 470 cm	0.2M HNO_3	-	-		-	-	0.282742 ± 20	-1.1	± 1.6	-	-
KZAI-01 - 560 cm	0.2M HNO_3	-	-		-	-	0.282746 ± 16	-0.9	± 1.6	-	-
KZAI-01 - 680 cm	HH	0.511822 ± 8	-15.88	± 0.27	-	-	-	-		-	-
'	0.2M HNO_3						0.282742 ± 13	-1.1	± 1.6	-	-
KZAI-01 - 688 cm	HH	0.511838 ± 13	-15.57	± 0.27	-	-	-	-		-	-
'	0.2M HNO_3	-	-		-	-	0.282742 ± 29	-1.1	± 1.6	-	-
Fine-grained sediments											
Congo fan											
KZAI-01 - 6 cm	Fusion	0.511812 ± 16	-16.07	± 0.31	32.6	5.9	0.282542 ± 8	-8.1	± 0.8	3.8	0.32
KZAI-01 - 41 cm	Fusion	0.511813 ± 19	-16.05	± 0.37	41.6	7.2	0.282530 ± 7	-8.6	± 0.8	4.0	0.34
KZAI-01 - 47 cm	Fusion	0.511799 ± 12	-16.33	± 0.27	40.0	7.0	0.282488 ± 13	-10.0	± 0.8	4.0	0.34
KZAI-01 - 241 cm	Fusion	0.511800 ± 10	-16.31	± 0.27	34.5	6.0	0.282570 ± 9	-7.1	± 0.8	4.0	0.30
KZAI-01 - 341 cm	Fusion	0.511799 ± 11	-16.33	± 0.27	26.9	4.5	-	-		3.9	0.28
KZAI-01 - 421 cm	Fusion	0.511827 ± 10	-15.78	± 0.27	27.8	4.7	0.282528 ± 8	-8.6	± 0.8	3.9	0.28
KZAI-01 - 470 cm	Fusion	0.511809 ± 6	-16.13	± 0.27	28.4	4.9	0.282427 ± 19	-12.2	± 0.8	4.1	0.29
KZAI-01 - 560 cm	Fusion	0.511833 ± 10	-15.66	± 0.27	25.0	4.3	0.282433 ± 8	-12.0	± 0.8	4.2	0.27
KZAI-01 - 680 cm	Fusion	0.511800 ± 11	-16.31	± 0.27	29.0	4.8	0.282448 ± 8	-11.5	± 0.8	4.1	0.28
KZAI-01 - 688 cm	Fusion	0.511802 ± 9	-16.27	± 0.27	27.7	4.6	0.282464 ± 11	-10.9	± 0.8	4.1	0.28
Angola and Cape basins											
MD96-2091 - 2 cm	Acid digestion	*0.511514 ± 6*	*-21.89*	*± 0.16*	*28.4*	4.9	0.282585 ± 11	-6.6	± 0.8	4.3	0.29
MD96-2098 - 0 cm	Acid digestion	*0.511972 ± 11*	*-12.95*	*± 0.21*	*12.0*	2.2	0.282610 ± 11	-5.7	± 0.8	2.1	0.22
MD96-2098 - 25 cm	Acid digestion	*0.511954 ± 8*	*-13.30*	*± 0.16*	*16.2*	3.1	0.282274 ± 14	-17.6	± 0.8	3.1	0.31
MD96-2098 - 110 cm	Acid digestion	*0.512022 ± 8*	*-11.98*	*± 0.16*	*8.5*	1.5	0.282585 ± 11	-6.6	± 0.8	1.9	0.16
MD96-2098 - 201 cm	Acid digestion	*0.512096 ± 8*	*-10.53*	*± 0.16*	*17.5*	3.6	0.282614 ± 12	-5.6	± 0.8	3.0	0.31
MD96-2098 - 231 cm	Acid digestion	*0.512095 ± 8*	*-10.55*	*± 0.16*	*17.3*	3.3	0.282630 ± 11	-5.0	± 0.8	3.3	0.28
MD96-2086 - 46 cm	Acid digestion	*0.512029 ± 6*	*-11.84*	*± 0.16*	*20.6*	3.6	0.282583 ± 26	-6.7	± 0.9	3.5	0.32
MD96-2086 - 161 cm	Acid digestion	*0.512130 ± 8*	*-9.87*	*± 0.16*	*23.5*	4.3	0.282705 ± 25	-2.4	± 0.9	3.9	0.39
MD96-2086 - 469 cm	Acid digestion	*0.512081 ± 5*	*-10.83*	*± 0.16*	*15.8*	3.1	0.282626 ± 14	-5.2	± 0.8	3.8	0.28
MD96-2086 - 748 cm	Acid digestion	*0.512080 ± 4*	*-10.85*	*± 0.16*	*16.4*	2.7	0.282625 ± 11	-5.2	± 0.8	4.5	0.32
MD96-2086 - 1009 cm	Acid digestion	*0.512059 ± 5*	*-11.26*	*± 0.16*	*16.3*	3.4	0.282615 ± 11	-5.5	± 0.8	4.3	0.31
MD96-2086 - 1072 cm	Acid digestion	*0.512243 ± 8*	*-7.67*	*± 0.16*	*10.5*	1.9	0.282612 ± 25	-5.6	± 0.9	4.4	0.27
MD96-2085 - 0 cm	Acid digestion	*0.512052 ± 14*	*-11.39*	*± 0.27*	*21.6*	4.4	0.282626 ± 10	-5.2	± 0.8	3.8	0.39
MD96-2085 - 110 cm	Acid digestion	*0.512134 ± 6*	*-9.79*	*± 0.16*	*21.5*	4.1	0.282635 ± 12	-4.8	± 0.8	4.5	0.43
MD96-2087 - 5 cm	Acid digestion	0.512009 ± 5	-12.23	± 0.16	15.6	3.1	0.282537 ± 12	-8.3	± 0.8	2.4	0.30
MD96-2087 - 229 cm	Acid digestion	0.512062 ± 5	-11.20	± 0.16	26.5	5.3	0.282556 ± 11	-7.6	± 0.8	5.0	0.54
MD96-2087 - 603 cm	Acid digestion	0.512108 ± 5	-10.30	± 0.16	20.7	4.5	0.282542 ± 11	-8.1	± 0.8	4.2	0.36
MD96-2087 - 890 cm	Acid digestion	0.512089 ± 4	-10.67	± 0.16	18.2	3.4	0.282610 ± 27	-5.7	± 0.9	3.6	0.32
MD96-2087 - 1201 cm	Acid digestion	0.512087 ± 8	-10.71	± 0.16	10.2	2.1	0.282600 ± 14	-6.1	± 0.8	2.0	0.18
Coarse-grained sediments (Congo canyon)											
KZAI-13 - 875 cm	Fusion	0.511815 ± 9	-16.02	± 0.21	14.8	2.9	0.282003 ± 8	-27.2	± 0.4	5.2	0.24
KZAI-05 - 1077 cm	Fusion	0.511807 ± 6	-16.17	± 0.21	27.1	5.2	0.281989 ± 7	-27.7	± 0.4	9.4	0.37
KZAI-08 - 515 cm	Fusion	0.511775 ± 9	-16.80	± 0.21	15.0	2.9	0.281879 ± 7	-31.6	± 0.4	10.3	0.32
KZAI-08 - 515 cm - repl.	Fusion	0.511768 ± 12	-16.93	± 0.21			0.281883 ± 5	-31.4	± 0.4		

The values of ε_{Hf} and ε_{Nd} represent the relative deviation of the $^{176}Hf/^{177}Hf$ and $^{143}Nd/^{144}Nd$ ratios of a sample, in parts per 10^4, from that of the CHUR reference (CHondritic Uniform Reservoir): $[(^{176}Hf/_{177}Hf)sample / (^{176}Hf/^{177}Hf)_{CHUR} -1] \times 10^4$. Here, ε_{Hf} and ε_{Nd} are calculated relative to $(^{176}Hf/^{177}Hf)_{CHUR} = 0.282772$ (Blichert-Toft and Albarède, 1997) and $(^{143}Nd/^{144}Nd)_{CHUR} = 0.512638$ (Jacobsen and Wasserburg, 1980).

Errors for εHf and εNd are reported as 2sd (external reproducibilty). When the in-run error (2se) is larger than 2sd, then error is given as 2se. Data in italics are from Bayon et al. (2003).

Figure1

Click here to download Figure: Fig1.pdf

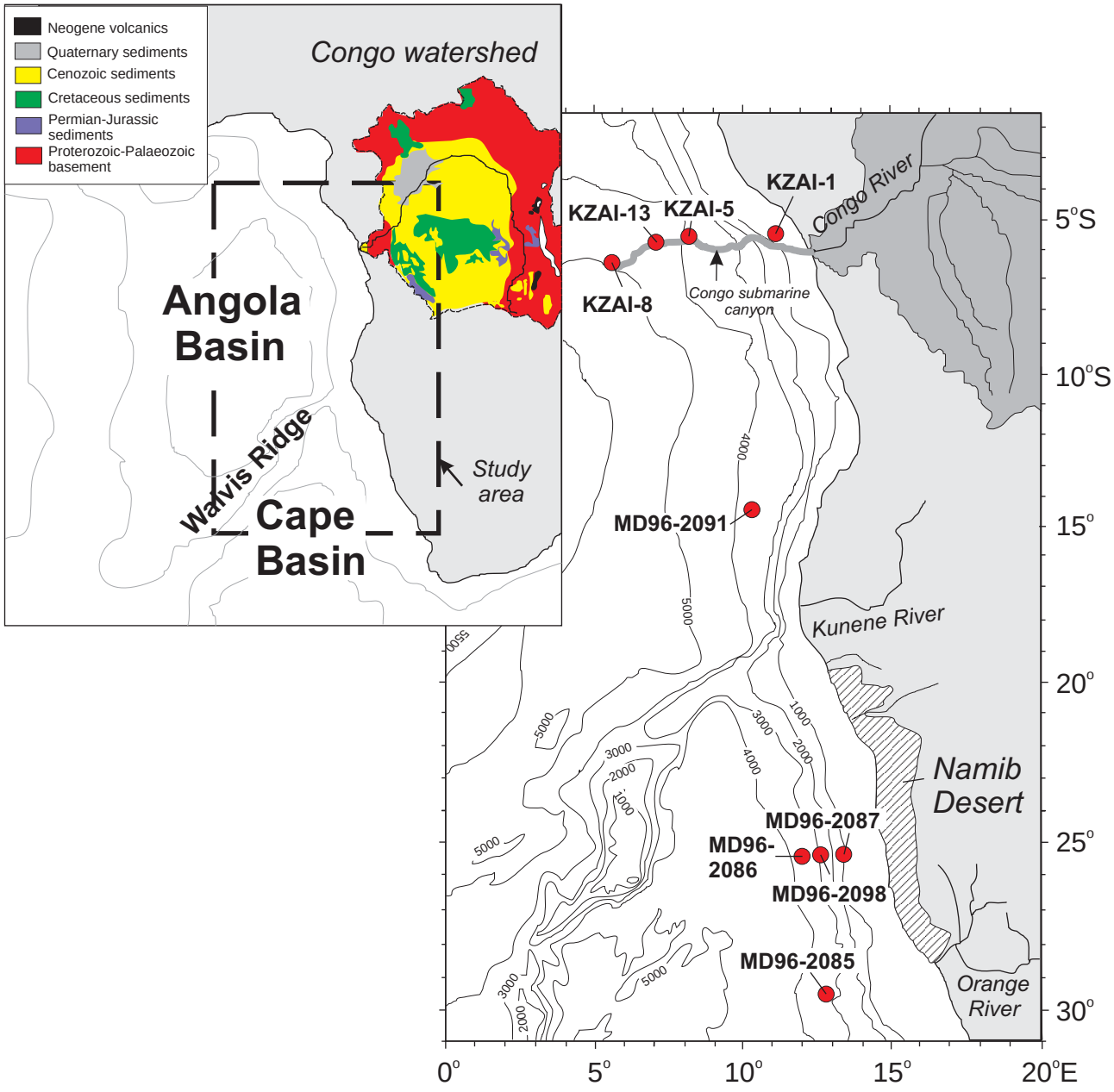

Fig 1

Figure2
Click here to download Figure: Fig2.pdf

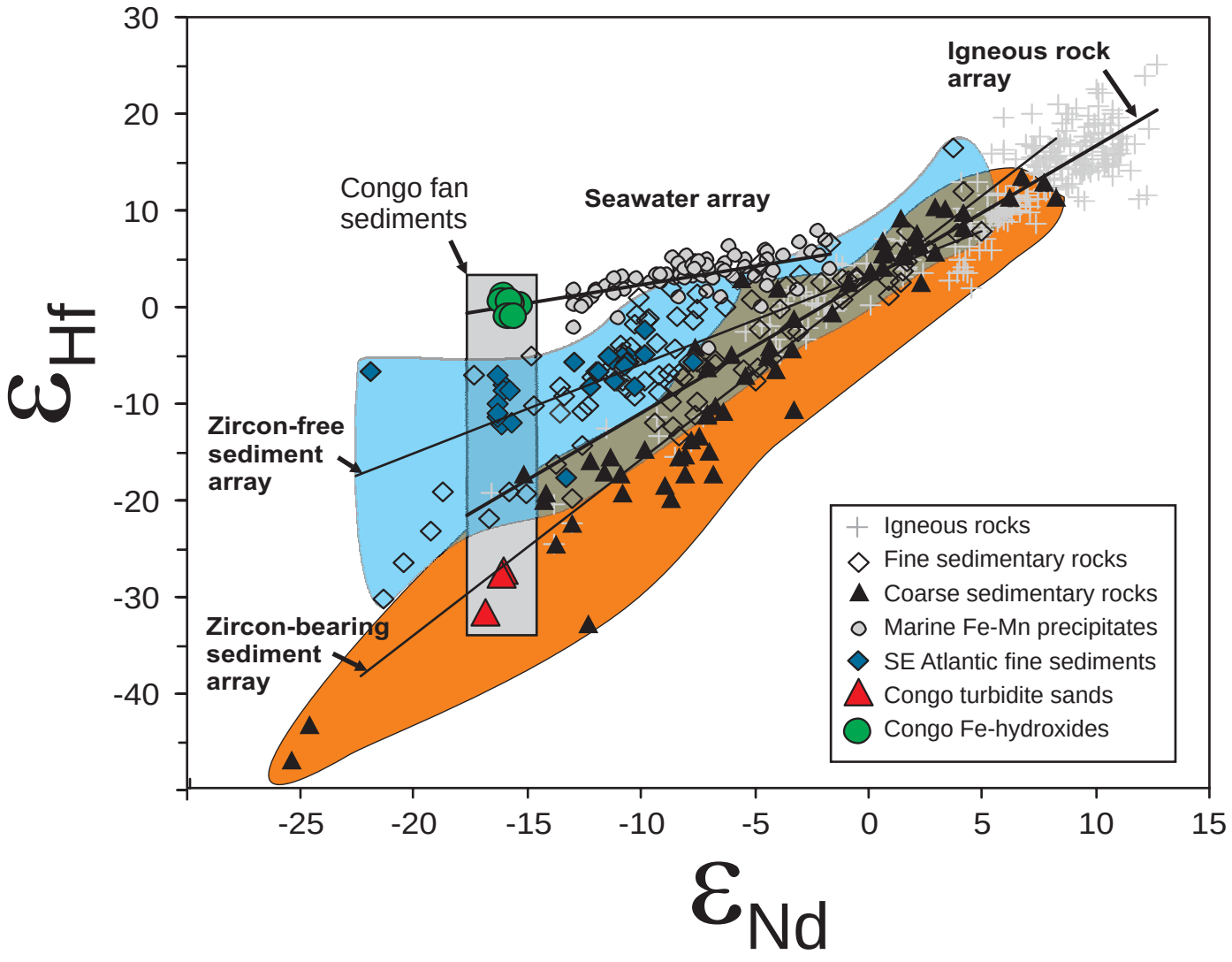

Fig 2

Figure3
Click here to download Figure: Fig3.pdf

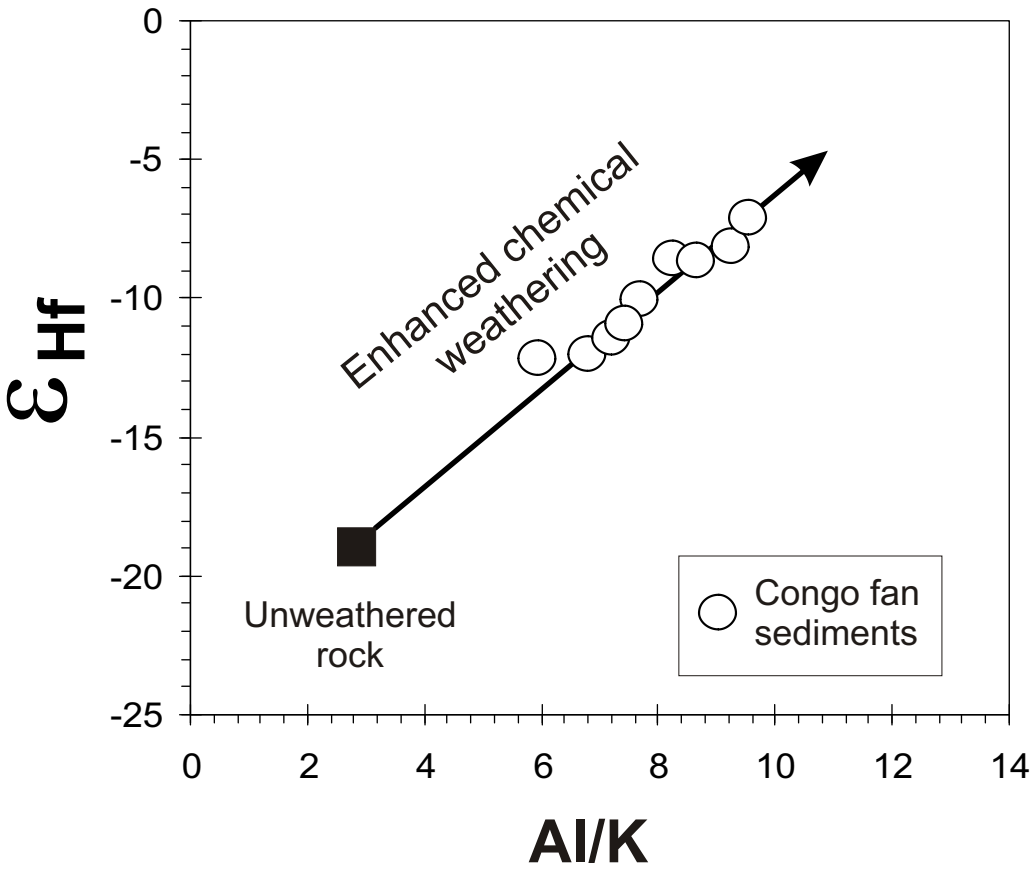

Fig 3

Figure4
Click here to download Figure: Fig4.pdf

(a)

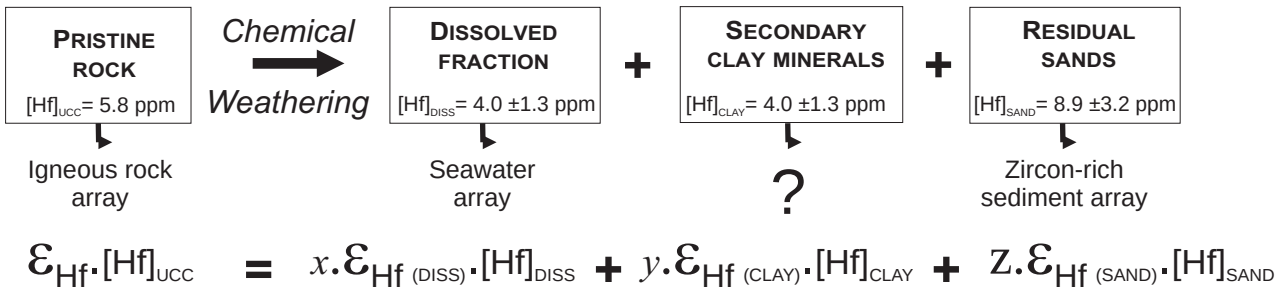

$$\varepsilon_{Hf}.[Hf]_{UCC} = x.\varepsilon_{Hf\ (DISS)}.[Hf]_{DISS} + y.\varepsilon_{Hf\ (CLAY)}.[Hf]_{CLAY} + z.\varepsilon_{Hf\ (SAND)}.[Hf]_{SAND}$$

(b)

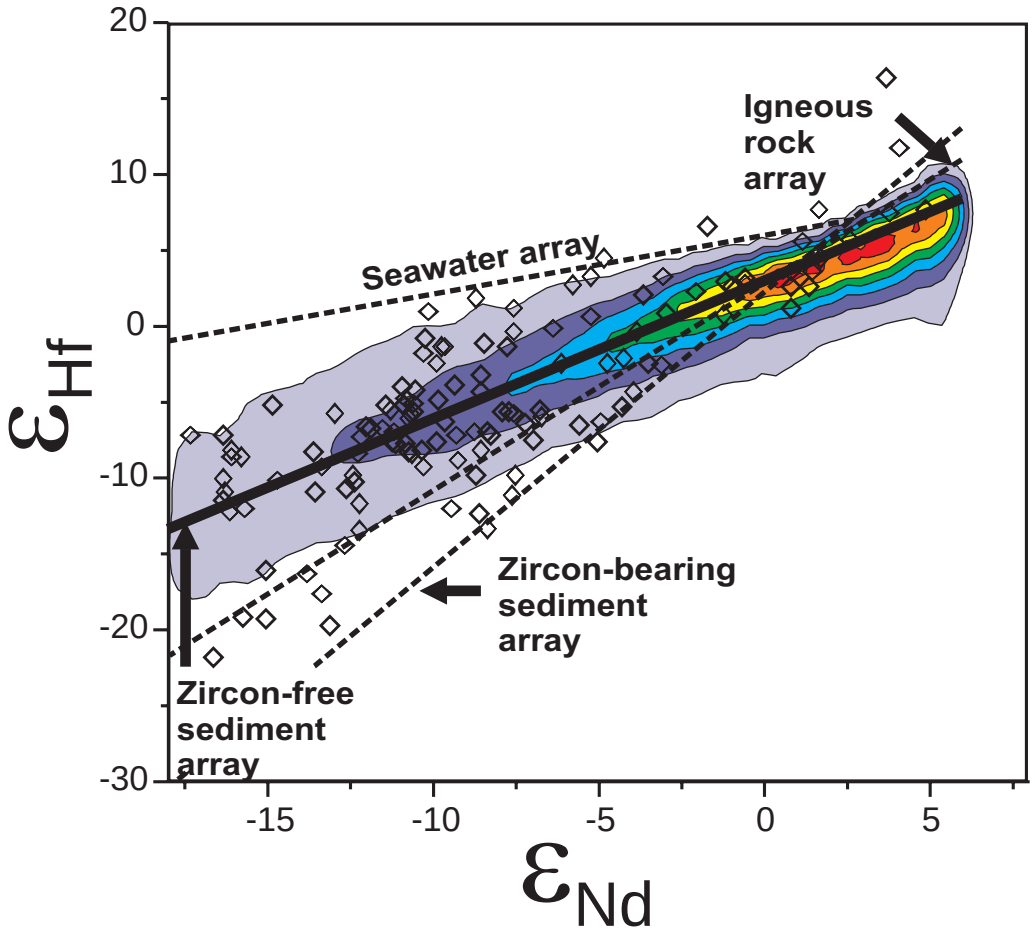

Fig 4